Science Advances
AAAS

Supplementary Materials for

Quantum control of flying doughnut terahertz pulses

Kamalesh Jana *et al.*

Corresponding author: Kamalesh Jana, kjana@uottawa.ca; Paul B. Corkum, pcorkum@uottawa.ca

Sci. Adv. **10**, eadl1803 (2024)
DOI: 10.1126/sciadv.adl1803

This PDF file includes:

Supplementary Text

1. Full experimental setup for current and THz measurements:

The full experimental setup is schematically depicted in Fig. S1(A). The two-colour (ω and 2ω) pulses are passed through an interferometer that allows relative phase to be adjusted by a piezo actuator. For the current measurements, flip mirror mount is positioned to reflect the combined ω and 2ω pulses. A focusing lens (f = 200 mm) is used to focus the combined pulses onto the LT-GaAs optoelectronic detector. The single pixel detector is raster scanned to measure the spatial distribution of the currents at image plane.

For THz measurements, flip mirror mount is set such that the two-colour pulses do not reflect from the mirror. The combined pulses are now gently focused (spot diameter of 700 μm) onto the 110-μm-thick GaAs substrate using a focusing lens to generate currents. The intensities of the ω and 2ω beams on the sample were 2 x 10^{11} W/cm^2 and 4 x 10^9 W/cm^2, respectively. THz pulses are radiated in both the backward and forward directions from the transient ring current. However, the THz pulse propagating through the thick GaAs substrate will be significantly suppressed by the free-carrier plasma generated by the ω beam. Therefore, we collect the THz pulse radiated from front side into air (reflection geometry) by a THz lens (f = 75 mm) and subsequently refocus it onto the electro-optic crystal (<110>-cut ZnTe) by another THz lens (f = 100 mm). In front of the first THz lens we place a 0.5-mm-thick uncoated germanium substrate to block the residual ω and 2ω pump pulses and filter out only THz pulses. We pinhole with the ZnTe crystal to spatially resolve the THz radiation. The assembly (ZnTe and pinhole) was placed on a two-dimensional (x-y) linear stage for raster scanning the probe. By doing this we rule out the additional effect in the measurements due to the non-uniformity of the ZnTe crystal. In order to mapout the far field spatial profiles of peak THz fields E_x (x, y) and E_y (x, y) we used a THz polarizer to select the polarization and raster scanned the pinhole across the probe. We also rotated the orientation of ZnTe crystal accordingly such that it measures E_x and E_y efficiently. THz is partly absorbed by the distributed water vapor present in the ambient air [Relative humidity (RH) 41%]. The THz part of the setup is enclosed and purged with dry air (achieved RH 12%) to reduce the water vapor absorption of THz pulse.

Peak THz field was calculated from the intensity modulation in balance detected EOS signal *(41) i.e.,* $\boldsymbol{sin^{-1}\left(\frac{\Delta I}{I}\right) = \frac{2\pi {n_0}^3 r_{41} t_{ZnTe} E_{THz} L}{\lambda_0}}$, where L is ZnTe thickness, r_{41} is EO coefficient of ZnTe, n_0 is the refractive index of ZnTe at probe wavelength, λ_0 is probe wavelength, t_{ZnTe} is coefficient of transmission. We also estimated peak THz electric field from the expression $\boldsymbol{E_{THz} = \sqrt{\frac{2W}{c\varepsilon_0 A\tau}}}$, where W is the THz pulse energy, c is the speed of light in vacuum, and ε_0 is the vacuum permittivity. While all the parameters are known here, the THz pulse energy is assumed to be 40 pJ considering 10^{-6} conversion efficiency (*42*). The estimated values of the THz peak field using these two methods really matches well.

2. Far-field profiles of the radiated THz pulse from radial current:

We measured spatial profiles *Ex (x, y)* and *Ey (x, y)* of the radiated electric field from the radial current. The spatial (x-y) maps of the electric fields were measured at the peak of the radiated THz pulse (Fig. S5). As we used <110>-faced ZnTe crystal we can only measure transverse profiles of the radial THz mode.

3. Optimization and direct measurement of THz magnetic field

In this section, we discuss how the radiated THz magnetic field can be increased. First, improving the collection and imaging efficiency of our optical system would considerably enhance the measured THz field. We use two THz lenses to collect and refocus the THz radiation. Having a first lens of F#3, does not collect the radiated light efficiently while with the second lens (F#4) we measure focused radiation with a focal spot diameter of 2.5 mm, thereby magnifying the 700 μm source by M=3.5. Finally, we filter out THz beam with 0.5 mm thick germanium substrate. The THz transmission of the germanium is ~ 40%. If the radiation were collected and imaged efficiently we predict that we would have measured ~10 mTesla for the peak magnetic field.

Second, if we enlarge the excitation area THz emission is increased. Efficient scaling of THz emission is possible as long as excitation power and spot size can be increased simultaneously. We have only used 50 μJ of the mJ 1.48 μm light available. By using more laser power and illuminating larger area while keeping the same power density, we will generate a larger THz field. For example, were we to irradiate a full 2.5 mm spot size keeping the same intensity, we predict a 3.6 times enhancement of radiated field reaching approximately 40 mTesla.

Third, using the nano-structured metals the THz magnetic field can be enhanced further. A factor of six enhancements was reported recently (*43*, *44*). Combining all these factors, we expect that it will be possible to generate a few 100 mT THz magnetic field from quantum-controlled currents excited in GaAs. Further enhancement will require other semiconductors or a more energetic 1.48 μm source. Tesla scale THz magnetic fields seem realistic from GaAs.

We also envisage that a terbium gallium garnet (TGG) crystal could be used in the place of ZnTe for direct measurement of the temporal structure of the THz magnetic field (*45*). The total Faraday rotation can be calculated using formula $\boldsymbol{\theta = VBL}$; where *V* is the Verdet constant of TGG, *B* is the magnetic field strength and *L* is the effective thickness of the TGG.

For our present experimental setup, 12 mm is the depth of the field (for 1 THz) and we predict θ =480 micro-radians**.** Although our current measurement uses electro-optic sampling and measures the maximum rotation of 100 milliradians, we have a signal to noise ratio of 250:1. Technically, we could resolve a rotation of 480 micro-radians and we could easily resolve a signal (with enhanced magnetic field) corresponding to 10 milliradians.

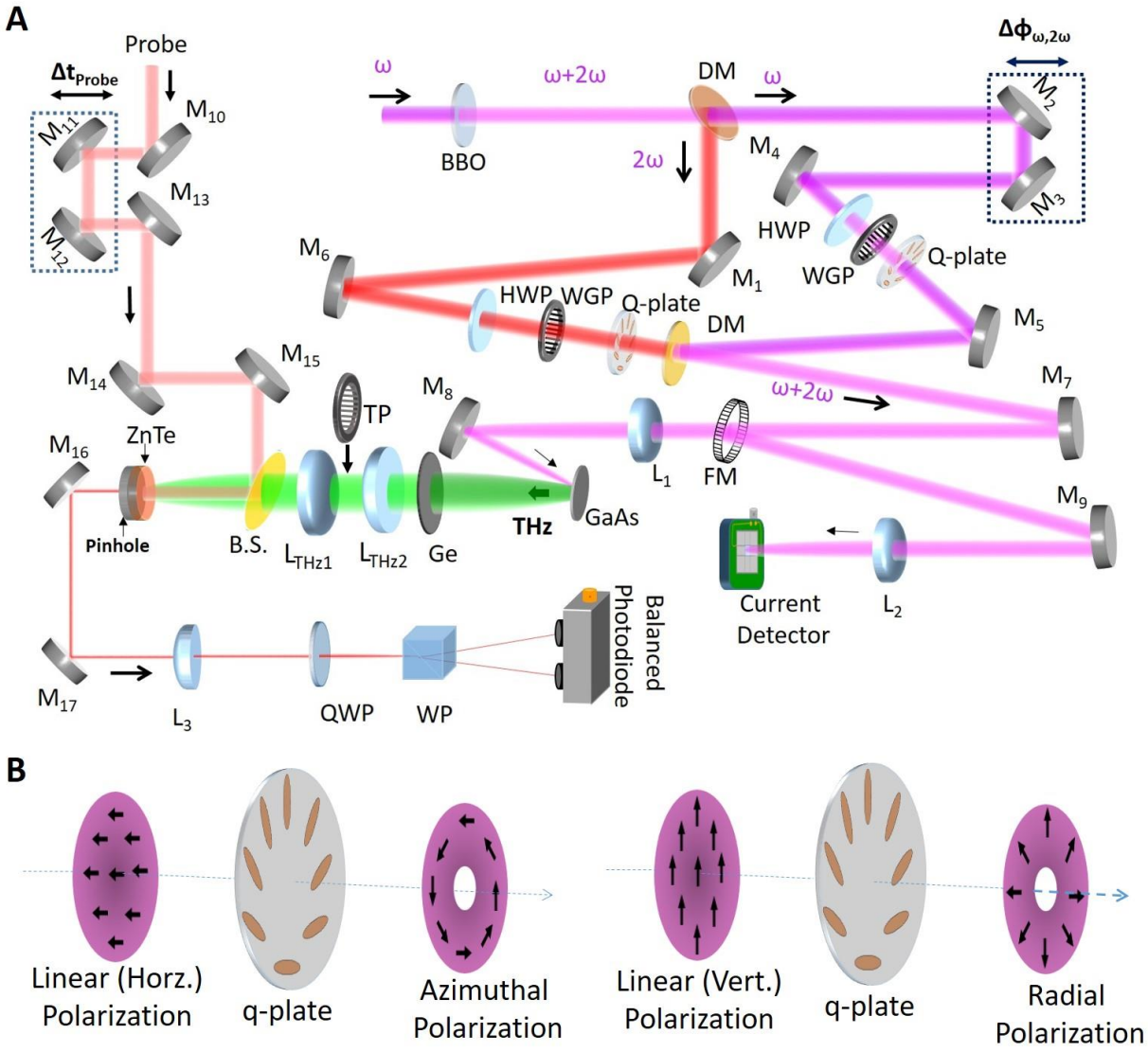

Fig. S1: Schematic of experimental setup for THz and current measurements. (A) Spatially filtered ω beam is passed through the BBO two generate 2ω pulse. Two pulses then travel through the two different arms of a two-colour interferometer and finally combined by a DM. BBO: beta-barium borate, DM: dichroic mirror, M_1-M_{17}: metallic mirrors, FM: flipper mirror, L_1-L_3: focussing lenses, L_{THz1}-L_{THz2}: THz lenses, TP: THz polarizer, HWP: half-wave plate, WGP: wire-grid polarizer, QWP: quarter-wave plate, WP: Wollaston prism, Q-plate: q-wave plate, GaAs: gallium arsenide substrate, Ge: germanium wafer, BS: pellicle beam splitter, ZnTe: Zinc telluride crystal. (B) Generation of azimuthal and radial polarizations from linear polarization using q-plate.

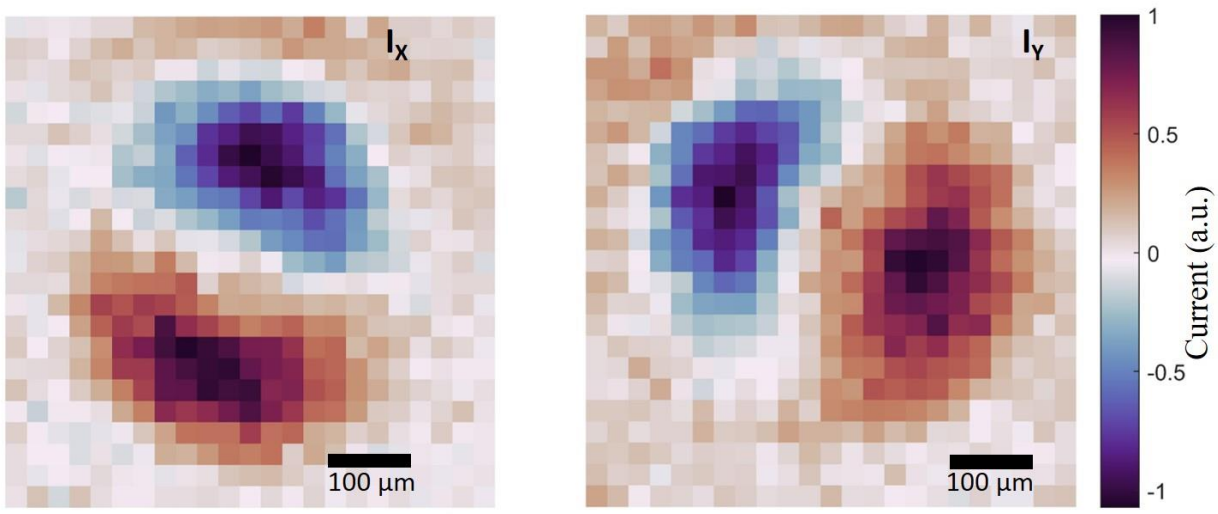

Fig. S2: Ring current measurement. Our LT-GaAs based current detector is direction sensitive. We measure the *x* (left) and *y* (right)-components of the current separately by rotating the detector accordingly. Combining the measured I_x and I_y enables spatial mapping of the ring current (presented in Fig. 1B).

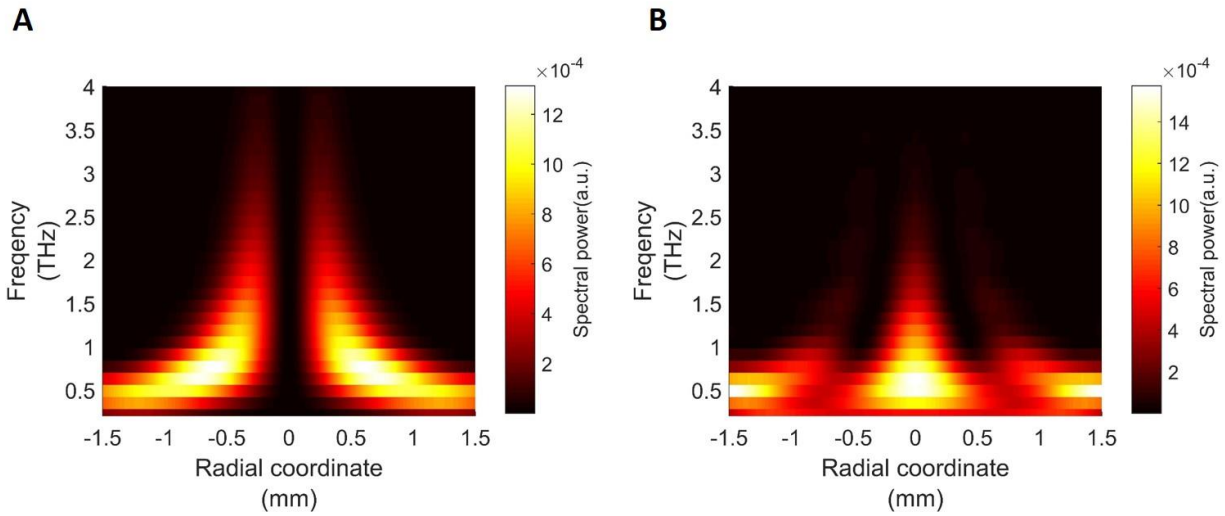

Fig. S3: Spatiospectral maps of the calculated electric and magnetic fields. We simulated the space-time structure of the radiated electric field (Fig. 1C) and magnetic field (Fig. 1D) from ring current. Space-frequency representation of the simulated (A) electric field and (B) magnetic field of the flying doughnut pulse from transient ring current are depicted.

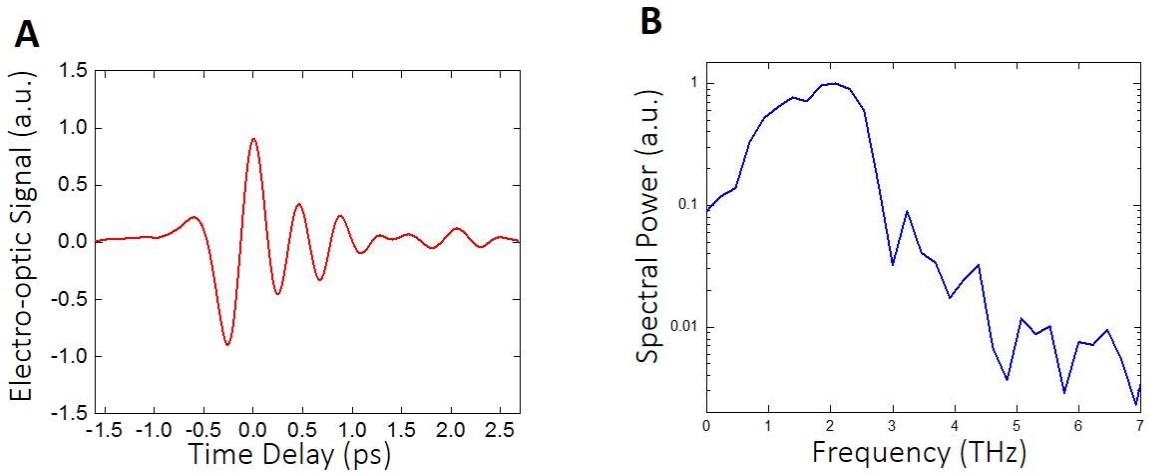

Fig. S4: THz pulse from GaAs under two-colour excitation. Rapidly oscillating two-colour injected current in GaAs radiates terahertz electromagnetic radiation. (A) Time-domain and (B) frequency domain representation of a typical THz waveform.

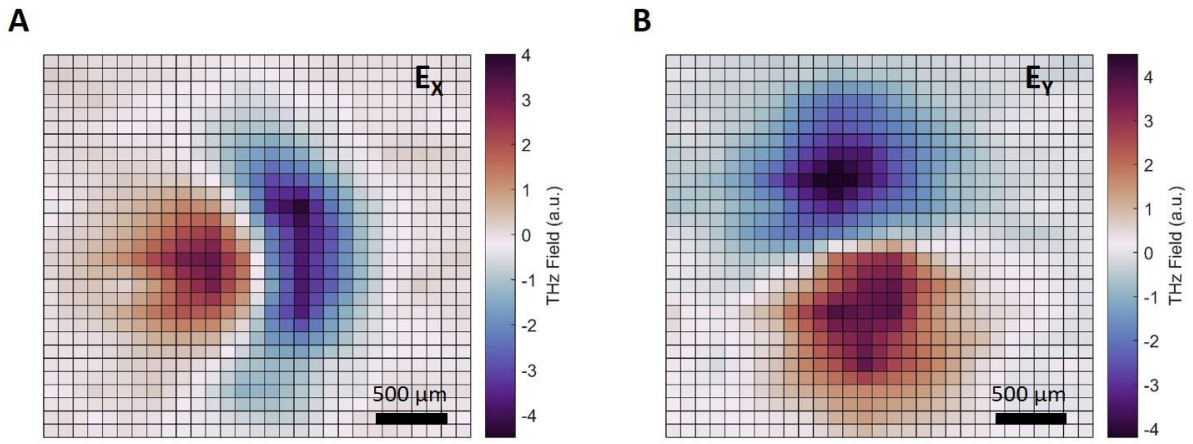

Fig. S5: Spatial profiles of THz pulse radiated from radial current. Spatial profiles of the two transverse components, (A) E_x (x, y) and (B) E_y (x, y) of the THz pulse radiated from radial current distribution.

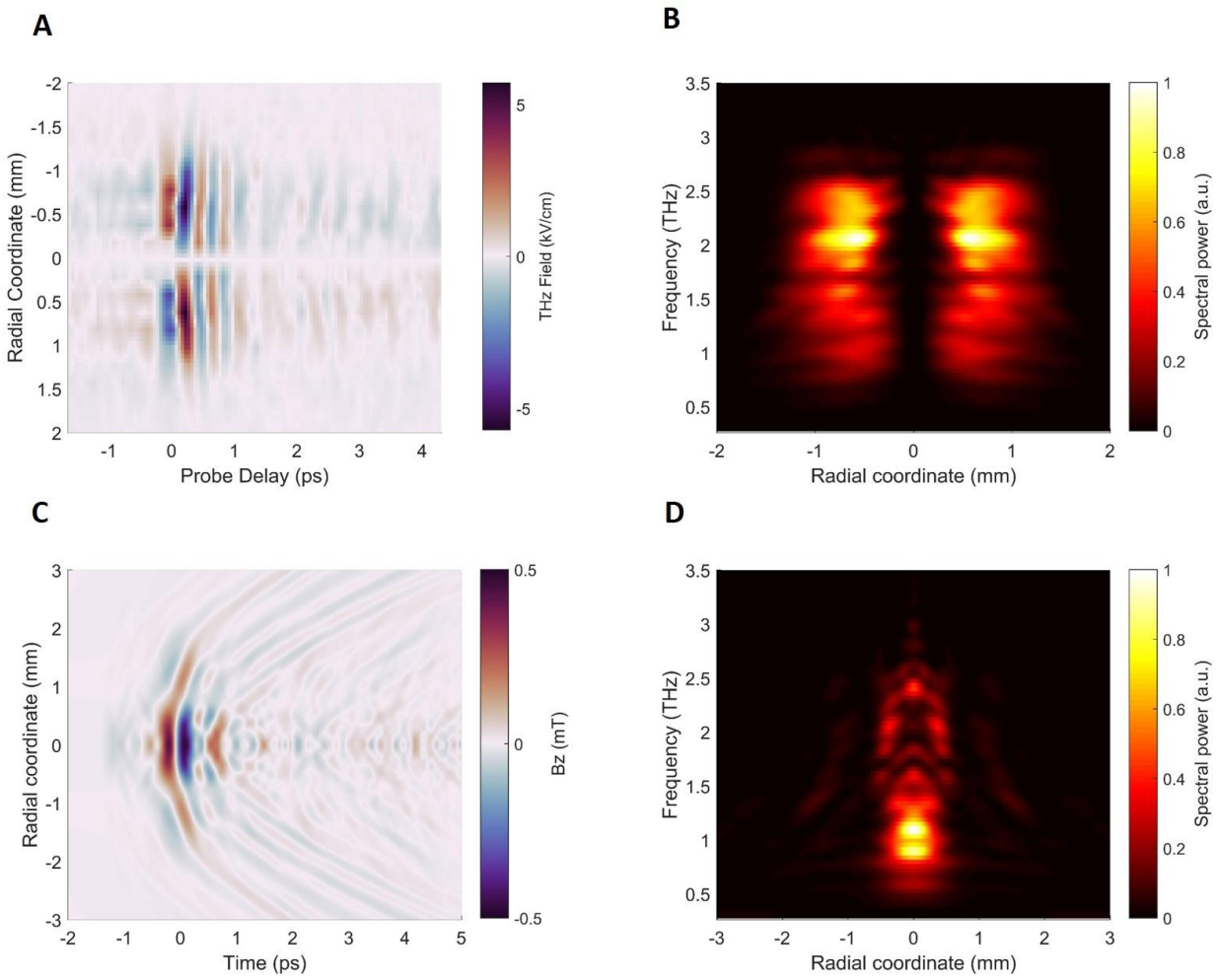

Fig. S6: Measurements of flying doughnut pulse in dry air (RH 12%) condition. (A) Measured electric field of flying doughnut pulses in dry air condition. (B) Space-frequency representation of the measured electric field. (C) Calculated magnetic field (B_z) structure of the flying doughnut pulse in dry air. (D) Spatiospectral map of the magnetic field B_z.

REFERENCES AND NOTES

1. H. Rubinsztein-Dunlop, A. Forbes, M. V. Berry, M. R. Dennis, D. L. Andrews, M. Mansuripur, C. Denz, C. Alpmann, P. Banzer, T. Bauer, E. Karimi, L. Marrucci, M. Padgett, M. Ritsch-Marte, N. M. Litchinitser, N. P. Bigelow, C Rosales-Guzmán, A. Belmonte, J. P. Torres, T. W. Neely, M. Baker, R. Gordon, A. B. Stilgoe, J. Romero, A. G. White, R. Fickler, A. E. Willner, G. Xie, B. McMorran, A. M. Weiner, Roadmap on structured light. *J. Opt.* **19**, 013001 (2016).

2. A. Forbes, Structured light: Tailored for purpose. *Opt. Photonics News* **31**, 24–31 (2020).

3. L. Lu, J. D. Joannopoulos, M. Soljačić, Topological photonics. *Nat. Photonics* **8**, 821–829 (2014).

4. T. Pu, J.-Y. Ou, V. Savinov, G. Yuan, N. Papasimakis, N. I. Zheludev, Unlabeled far-field deeply subwavelength topological microscopy (DSTM). *Adv. Sci.* **8**, 20022886 (2020).

5. Y. Dai, Z. Zhou, A. Ghosh, R. S. K. Mong, A. Kubo, C. B. Huang, H. Petek, Plasmonic topological quasiparticle on the nanometre and femtosecond scales. *Nature* **588**, 616–619 (2020).

6. Z. Zhang, X. Qiao, B. Midya, K. Liu, J. Sun, T. Wu, W. Liu, R. Agarwal, J. M. Jornet, S. Longhi, N. M. Litchinitser, L. Feng, Tunable topological charge vortex microlaser. *Science* **368**, 760–763 (2020).

7. R. W. Hellwarth, P. Nouchi, Focused one-cycle electromagnetic pulses. *Phys. Rev. E* **54**, 889–895 (1996).

8. A. Zdagkas, C. McDonnell, J. Deng, Y. Shen, G. Li, T. Ellenbogen, N. Papasimakis, N. I. Zheludev, Observation of toroidal pulses of light. *Nat. Photonics* **16**, 523–528 (2022).

9. N. Papasimakis, T. Raybould, V. A. Fedotov, D. P. Tsai, I. Youngs, N. I. Zheludev, Pulse generation scheme for flying electromagnetic doughnuts. *Phys. Rev. B* **97**, 201409 (2018).

10. M. Koch, D. M. Mittleman, J. Ornik, E. Castro-Camus, Terahertz time-domain spectroscopy. *Nat. Rev. Methods Primers* **3**, 48 (2023).

11. S. Keren-Zur, M. Tal, S. Fleischer, D. M. Mittleman, T. Ellenbogen, Generation of spatiotemporally tailored terahertz wavepackets by nonlinear metasurfaces. *Nat. Commun.* **10**, 1778 (2019).

12. L. Luo, I. Chatzakis, J. Wang, F. B. P. Niesler, M. Wegener, T. Koschny, C. M. Soukoulis, Broadband terahertz generation from metamaterials. *Nat. Commun.* **5**, 3055 (2014).

13. X. C. Zhang, D. H. Auston, Optically induced THz electromagnetic radiation from planar photoconducting structures. *J. Electromagn. Waves Appl.* **6**, 85–106 (1992).

14. E. Dupont, P. B. Corkum, H. C. Liu, M. Buchanan, Z. R. Wasilewksi, Phase-controlled currents in semiconductors. *Phys. Rev. Lett.* **74**, 3596–3599 (1995).

15. R. Atanasov, A. Haché, J. L. P. Hughes, H. M. van Driel, J. E. Sipe, Coherent control of photocurrent Generation in bulk semiconductors. *Phys. Rev. Lett.* **76**, 1703–1706 (1996).

16. M. Shapiro, P. Brumer, *Quantum Control of Molecular Processes* (John Wiley & Sons, 2011).

17. S. Sederberg, F. Kong, F. Hufnagel, C. Zhang, E. Karimi, P. B. Corkum, Vectorized optoelectronic control and metrology in a semiconductor. *Nat. Photonics* **14**, 680–685 (2020).

18. K. Jana, K. R. Herperger, F. Kong, Y. Mi, C. Zhang, P. B. Corkum, S. Sederberg, Reconfigurable electronic circuits for magnetic fields controlled by structured light. *Nat. Photonics* **15**, 622–626 (2021).

19. K. Jana, E. Okocha, S. H. Møller, Y. Mi, S. Sederberg, P. B. Corkum, Reconfigurable terahertz metasurfaces coherently controlled by wavelength-scale-structured light. *Nanophotonics* **11**, 787–795 (2022).

20. S. Sederberg, P. B. Corkum, Perspective on phase-controlled currents in semiconductors driven by structured light. *Appl. Phys. Lett.* **120**, 160504 (2022).

21. H. Larocque J. Gagnon-Bischoff, F. Bouchard, R. Fickler, J. Upham, R. W. Boyd, E. Karimi, Arbitrary optical wavefront shaping via spin-to-orbit coupling, *J. Opt.* **18**, 124002 (2016).

22. N. I. Zheludev, D. Wilkowski, The rise of toroidal electrodynamics and spectroscopy. *ACS Photonics* **10**, 556–558 (2023).

23. I. Kuprov, D. Wilkowski, N. Zheludev, Toroidal optical transitions in hydrogen-like atoms. *Sci. Adv.* **8**, eabq6751 (2022).

24. T. A. Raybould, V. A. Fedotov, N. Papasimakis, I. Kuprov, I. J. Youngs, W. T. Chen, D. P. Tsai, N. I. Zheludev, Toroidal circular dichroism. *Phys. Rev. B* **94**, 035119 (2016).

25. S. Sederberg, F. Kong, P. B. Corkum, Tesla-scale terahertz magnetic impulses. *Phys. Rev. X* **10**, 011063 (2020).

26. S. Wang, Y. Bai, P. Liu, Generation of terahertz spatiotemporal optical vortices with frequency-dependent orbital angular momentum. *Opt. Express* **31**, 16267–16280 (2023).

27. Y. Mi, K. Johnston, V. Shumakova, S. H. Møller, K. Jana, C. Zhang, A. Staudte, S. Sederberg, P. B. Corkum, Active stabilization of terahertz waveforms radiated from a two-color air plasma. *Photonics Res.* **10**, 96–103 (2022).

28. A. Kirilyuk, A. V. Kimel, T. Rasing, Ultrafast optical manipulation of magnetic order. *Rev. Mod. Phys.* **82**, 2731–2784 (2010).

29. K. Yamaguchi, M. Nakajima, T. Suemoto, Coherent control of spin precession motion with impulsive magnetic fields of half-cycle terahertz radiation. *Phys. Rev. Lett.* **105**, 237201 (2010).

30. K. Yamaguchi, T. Kurihara, Y. Minami, M. Nakajima, T. Suemoto, Terahertz time-domain observation of spin reorientation in orthoferrite ErFeO3 through magnetic free induction decay. *Phys. Rev. Lett.* **110**, 137204 (2013).

31. I. Tudosa, C. Stamm, A. B. Kashuba, F. King, H. C. Siegmann, J. Stöhr, G. Ju, B. Lu, D. Weller, The ultimate speed of magnetic switching in granular recording media. *Nature* **428**, 831–833 (2004).

32. T. Higuchi, C. Heide, K. Ullmann, H. B. Weber, P. Hommelhoff, Light-field-driven currents in graphene. *Nature* **550**, 224–228 (2017).

33. D. Sun, C. Divin, J. Rioux, J. E. Sipe, C. Berger, W. A. Heer, P. N. First, T. B. Norris, Coherent control of ballistic photocurrents in multilayer epitaxial graphene using quantum interference. *Nano Lett.* **10**, 1293–1296 (2010).

34. F. Kong, H. Larocque, E. Karimi, P. B. Corkum, C. Zhang, Generating few-cycle radially polarized pulses. *Optica* **6**, 160–164 (2019).

35. D. Haberberger, S. Tochitsky, C. Joshi, Fifteen terawatt picosecond CO_2 laser system. *Opt. Express* **18**, 17865–17875 (2010).

36. M. N. Polyanskiy, I. V. Pogorelsky, M. Babzien, R. Kupfer, K. L. Vodopyanov, M. A. Palmer, Post-compression of long-wave infrared 2 picosecond sub-terawatt pulses in bulk materials. *Opt. Express* **29**, 31714–31725 (2021).

37. P. B. Corkum, Amplification of picosecond 10 μm pulses in multiatmosphere CO2 lasers *IEEE J. Quantum Electron.* **21**, 216–232 (1985).

38. M. N. Polyanskiy, I. V. Pogorelsky, M. Babzien, R. Kupfer, N. Vafaei-Najafabadi, M. A. Palmer, High-peak-power long-wave infrared lasers with CO_2 amplifiers. *Photonics* **8**, 101 (2021).

39. S. Carbajo, E. Granados, D. Schimpf, A. Sell, K. H. Hong, J. Moses, F. X. Kärtner, Efficient generation of ultra-intense few-cycle radially polarized laser pulses. *Opt. Lett.* **39**, 2487–2490 (2014).

40. P. Schmelcher, L. S. Cederbaum, in *High Magnetic Fields: Science and Technology*, vol. 2, F. Herlach, N. Miura, Eds. (World Scientific, 2003), pp. 245–266.

41. M. C. Hoffmann, S. Schulz, S. Wesch, S. Wunderlich, A. Cavalleri, B. Schmidt, Coherent single-cycle pulses with MV/cm field strengths from a relativistic transition radiation light source. *Opt. Lett.* **36**, 4473–4475 (2011).

42. D. Côté, J. M. Fraser, M. DeCamp, P. H. Bucksbaum, H. M. van Driel, THz emission from coherently controlled photocurrents in GaAs. *Appl. Phys. Lett.* **75**, 3959–3961 (1999).

43. M. Blanco, F. Cambronero, M. T. Flores-Arias, E. C. Jarque, L. Plaja, C. Hernández-Garcíaet, Ultraintense femtosecond magnetic nanoprobes induced by azimuthally polarized laser beams. *ACS Photonics* **6**, 38–42 (2019).

44. D. Polley, N. Z. Hagström, C. von Kroff Schmising, S. Eisebitt, S. Bonetti, Terahertz magnetic field enhancement in an asymmetric spiral metamaterial. *J. Phys. B At. Mol. Opt. Phys.* **51**, 224001 (2018).

45. J. A. Riordan, F. G. Sun, Z. G. Lu, X.-C. Zhang, Free-space transient magneto-optic sampling. *Appl. Phys. Lett.* **71**, 1452–1454 (1997).